SCIENCE CHINA
Chemistry

• ARTICLES •
• SPECIAL ISSUE • Chemical Methodology

January 2014 Vol.57 No.1: 107–113
doi: 10.1007/s11426-013-5012-8

Synthesis, structure and property of one porous Zn(salen)-based metal-metallosalen framework

PENG YongWu[1†], ZHU ChengFeng[1,2†] & CUI Yong[1*]

[1]*State Key Laboratory of Metal Matrix Composites; School of Chemistry and Chemical Engineering, Shanghai Jiao Tong University, Shanghai 200240, China*
[2]*School of Chemical Engineering, Hefei University of Technology, Hefei 230009, China*

Received August 8, 2013; accepted August 15, 2013; published online October 31, 2013

Chiral Schiff-base ligand **L** was synthesized through six steps in good overall yield from readily available 2-*tert*-butylphenol and was used to construct one chiral porous metal-metallosalen framework, $[Zn_5(\mu_3\text{-}OH)_2(ZnL)_4(H_2O)_2]\cdot 18H_2O$ (**1**, **L** = 5′,5″-(1*E*, 1′*E*)-(1*R*, 2*R*)-cyclohexane-1,2-diylbis(azan-1-yl-1-ylidene)bis(methan-1-yl-1-ylidene)bis(3′-*tert*-butyl-4′-hydroxybiphenyl-4-carboxylic acid), under mild reaction conditions. **1** was characterized by IR, TGA, CD, UV, PL, single-crystal and powder X-ray crystallography. The structure of **1** displays a 3-fold interpenetrating 3D framework with 1D channel of 1.14 nm × 0.58 nm and imparts unique Zn(salen) units on the surface of the pore, in which $(Zn\mathbf{L})_2$ dimer acts as multi-functionlized metalloligand. **1** is thermally robust with network decomposition temperature of 400 °C and it also exhibits strong photoluminescence in the visible region.

Schiff-base, metal-metallosalen framework, photoluminescence

1 Introduction

Metal-organic frameworks (MOFs) are crystalline porous hybrid solids composed of organic struts and inorganic nodes, and have attracted growing interest because of their intriguing architectures and topologies and promising applications in diverse areas such as gas storage, catalysis, separation and chemical sensing [1–9]. Unlike traditional inorganic materials, these materials feature structural diversity and amenability to be designed with desired functionalities at the molecular level [10–13]. Carboxyl-based ligands have been proved very useful building blocks to form porous MOFs and numerous novel structures with fascinating topologies and properties have been constructed with this kind of ligands [14–15]. On the other hand, Salen ligands and their metal complexes have been established as one of the best known privileged ligands and have been widely applied in asymmetric synthesis and separation, but less attention has been given to assemble salen or metallosalens into crystalline infinite solids [16–21]. We have recently utilized dicarboxyl-functionalized salen ligands to make several 3D porous MOFs, which exhibit unique properties on chemical sensor and asymmetric catalysis [22–23]. Encouraged by the successful construction of the aforementioned functional porous metal-metallosalen frameworks and to further extend our work in this field, herein we synthesize a C_2-symmetric salen ligand **L** and employ it to assemble with zinc ions to afford a porous metal-metallosalen framework **1**, and its structure, thermal stability and photoluminescence were studied.

2 Experimental

2.1 Materials and apparatus

All of the chemicals are commercial available, and used

*Corresponding author (email: yongcui@sjtu.edu.cn)
†These authors contributed equally to this work

without further purification. The IR (KBr pellet) spectra were recorded (400–4000 cm^{-1} region) on a Nicolet Magna 750 FT-IR spectrometer. Thermogravimetric analyses (TGA) were carried out in an N_2 atmosphere with a heating rate of 10 °C min^{-1} on a STA449C integration thermal analyzer. All UV-vis absorption spectra were recorded on a Lambda 20 UV-vis Spectrometer (Perkin Elmer, Inc., USA). The fluorescence spectra were carried out on a LS 50B Luminescence Spectrometer (Perkin Elmer, Inc., USA). The CD spectra were recorded on a J-800 spectropolarimeter (Jasco, Japan).

2.2 Crystallographic measurements and structure determination

Single-crystal XRD data for the compound was collected on a Bruker SMART Apex II CCD-based X-ray diffractometer with Cu-Kα radiation (λ = 1.54178 Å) for **1** at 173(2) K. In the range of 2.47º ⩽ θ ⩽ 68.36º, a total of 91529 reflections were collected and 52460 were independent with R_{int} = 0.0484, of which 30905 were observed with $I > 2\sigma(I)$. The structure was solved by direct methods with SHELXS-97 and refined with SHELXL-97 [24]. All the non-hydrogen atoms were refined by full-matrix techniques with anisotropic displacement parameters. The hydrogen atoms were geometrically fixed at calculated positions attached to their parent atoms, and treated as riding atoms. The crystallographic data and other pertinent information of complex **1** are summarized in Table 1, and the selected bond lengths and bond angles are given in Table 2.

Table 1 Crystal data for the title compound

Complex	**1**
Empirical formula	$C_{168}H_{168}N_8O_{48}Zn_9$
Formula weight	3655.43
Radiation (CuKα) (Å)	1.54178
Crystal system, Space group	Monoclinic, C_2
T (K)	100(2)
a (Å)	37.1058(19)
b (Å)	26.3491(12)
c (Å)	37.4578(18)
β (º)	105.311(3)
V (Å^3)	35323(3)
Z	4
D_c (g/cm^3)	0.0687
μ(CuKα) (cm^{-1})	0.994
F(000)	7544
θ range for data collection (°)	2.47 to 68.36
Index ranges	$-44 \le h \le 42, -30 \le k \le 31, -44 \le l \le 43$
Reflections collected/unique	91529/52460 (R_{int} = 0.0484)
Goodness-of-fit on F^2	1.097
Completeness to theta	96.7% (68.36 º)
R, wR ($I > 2\sigma(I)$)	R_1 = 0.1106, wR_2 = 0.2773
Flack parameter	–0.05(3)

2.3 Synthesis of ligand

The dicaxboxyl-functionalized Schiff-base ligand 5′,5″-(1*E*, 1′*E*)-(1*R*,2*R*)-cyclohexane-1,2-diyl-bis(azan-1-yl-1-ylidene) bis(methan-1-yl-1-ylidene)bis(3′-*tert*-butyl-4′-hydroxybiphenyl-4-carboxylic acid) (H_4**L**) was prepared in six steps in an overall 50% yield from 2-*tert*-butylphenol according to the reported procedures (Scheme 1) [18, 25]. IR (KBr, cm^{-1}): 3413 (w), 2942 (s), 2863 (m), 2669 (w), 2551 (w), 1684 (s), 1629 (s), 1607 (s), 1565(w), 1514 (w), 1469 (w), 1441 (s), 1422 (s), 1393 (m), 1361 (w), 1316 (m), 1292 (s), 1276 (s), 1254 (m), 1223 (w), 1176 (m), 1131 (w), 1101 (w), 1069 (w), 1039 (w), 1015 (w), 974 (w), 936 (w), 888 (w), 857 (m), 804 (w), 776 (m), 747 (w), 715 (w), 552 (w), 497 (w).

2.4 Synthesis of complex 1

The ligand (0.0033 g, 0.005 mmol), $Zn(NO_3)_2{\cdot}6H_2O$ (0.0029 g, 0.010 mmol), DMF (0.3 mL), MeOH (0.1 mL) and THF (0.1 mL) were added to a small vial that was sealed and heated to 373 K for one day and then cooled to room temperature. Yellow block-like crystals of **1** were filtered, washed with DMF and MeOH, respectively, and dried at room temperature. The yield based on the chiral ligand is up to 69.0%. IR (KBr, cm^{-1}): 3397 (w), 2938 (m), 2862 (m), 1663 (m), 1596(s), 1531 (s), 1462 (w), 1399 (s), 1385 (s), 1329 (m), 1277 (m), 1253 (m), 1230 (w), 1198 (w), 1183 (w), 1162 (s), 1084 (w), 1068 (m), 1036 (w), 1013 (w), 980 (w), 929 (w), 894 (w), 856 (m), 811 (w), 787 (m), 769 (m), 724 (w), 705 (w), 662 (w), 553 (w), 512 (m), 486 (w).

3 Results and discussion

3.1 Synthesis and characterization

The zinc (II) complex, **1**, was synthesized under mild reaction condition. Its bulk product was obtained by repeating the experiment and the resulted crystals were collected by filtration, washed several times with DMF and MeOH, and dried under vacuum for 3 h. Phase purity of the bulk sample was established by comparison of its observed and simulated powder X-ray diffraction patterns (PXRD) (Figure 1). The thermal stability of **1** was investigated on crystalline samples under a N_2 atmosphere from 40 to 800 ºC. TGA result of **1** shows that included guest molecules could be readily released in the temperature range from 80 to 260 ºC and the framework is stable up to ~400 ºC (Figure 2). Infrared spectrum of the complex **1** show that the carboxylate groups are coordinated to Zn^{2+} ions, as evidenced by a shift of the carboxylate stretching frequency from 1684 cm^{-1} in the protonated salen precursor H_4**L** to 1531 cm^{-1}, which is consistent with the structural results. The characteristic peaks at 1399 and 1385 cm^{-1} may come from C=N vibration, and the peaks at 2938 and 2862 cm^{-1} may be due to the

Table2 Selected bond lengths (Å) and bond angles (°)

Complex	**1**							
Bond	Dist.	Bond	Dist.	Bond	Dist.	Bond	Dist.
Zn(1)–O(10)	1.894(6)	Zn(4)–O(17)	1.893(6)	Zn(7)–O(15)#1	1.916(7)	Zn(10)–O(27)	1.908(8)
Zn(1)–O(9)	1.907(7)	Zn(4)–N(7)	1.991(6)	Zn(7)–O(13)#3	1.948(6)	Zn(10)–O(27)#4	1.908(8)
Zn(1)–N(4)	1.981(9)	Zn(4)–N(6)	1.992(8)	Zn(7)–O(13)	1.948(6)	Zn(10)–O(7)	1.998(10)
Zn(1)–N(2)	1.998(8)	Zn(5)–O(16)#1	1.905(9)	Zn(8)–O(20)	1.911(9)	Zn(10)–O(7)#4	1.998(10)
Zn(2)–O(4)	1.884(7)	Zn(5)–O(11)	1.950(7)	Zn(8)–O(8)#4	1.931(11)	O(6)–Zn(6)#3	1.907(9)
Zn(2)–O(3)	1.894(8)	Zn(5)–O(22)#2	1.972(6)	Zn(8)–O(2)	1.996(7)	O(8)–Zn(8)#4	1.931(11)
Zn(2)–N(3)	2.002(7)	Zn(5)–O(14)	2.114(1)	Zn(8)–O(27)	2.100(8)	O(15)–Zn(7)#5	1.916(7)
Zn(2)–N(1)	2.041(8)	Zn(5)–O(13)	2.118(7)	Zn(8)–O(28)	2.147(14)	O(16)–Zn(5)#6	1.905(9)
Zn(3)–O(24)	1.905(6)	Zn(6)–O(6)#3	1.907(9)	Zn(9)–O(25)#4	1.903(7)	O(21)–Zn(6)#5	1.939(6)
Zn(3)–O(23)	1.911(7)	Zn(6)–O(21)#2	1.939(6)	Zn(9)–O(1)	1.950(7)	O(22)–Zn(5)#5	1.972(6)
Zn(3)–N(8)	1.970(8)	Zn(6)–O(12)	1.943(7)	Zn(9)–O(19)	1.955(6)	O(25)–Zn(9)#4	1.903(7)
Zn(3)–N(5)	1.989(8)	Zn(6)–O(13)	1.975(6)	Zn(9)–O(27)	1.973(9)		
Zn(4)–O(18)	1.883(7)	Zn(7)–O(15)#2	1.916(7)	Zn(7)–O(15)#1	1.916(7)		
Angle	(°)	Angle	(°)	Angle	(°)	Angle	(°)
O(10)–Zn(1)–O(9)	116.2(3)	O(18)–Zn(4)–O(17)	115.6(3)	O(21)#2–Zn(6)–O(12)	108.9(3)	O(2)–Zn(8)–O(28)	88.7(5)
O(10)–Zn(1)–N(4)	108.7(3)	O(18)–Zn(4)–N(7)	97.4(3)	O(6)#3–Zn(6)–O(13)	124.4(4)	O(27)–Zn(8)–O(28)	176.2(6)
O(9)–Zn(1)–N(4)	98.8(3)	O(17)–Zn(4)–N(7)	109.9(3)	O(21)#2–Zn(6)–O(13)	105.3(2)	O(25)#4–Zn(9)–O(1)	105.5(3)
O(10)–Zn(1)–N(2)	98.5(3)	O(18)–Zn(4)–N(6)	110.9(3)	O(12)–Zn(6)–O(13)	100.0(3)	O(25)#4–Zn(9)–O(19)	106.7(4)
O(9)–Zn(1)–N(2)	110.2(4)	O(17)–Zn(4)–N(6)	98.1(3)	O(15)#2–Zn(7)–O(15)#1	112.7(5)	O(1)–Zn(9)–O(19)	122.8(3)
N(4)–Zn(1)–N(2)	125.6(3)	N(7)–Zn(4)–N(6)	126.0(3)	O(15)#2–Zn(7)–O(13)#3	108.4(4)	O(25)#4–Zn(9)–O(27)	123.7(4)
O(4)–Zn(2)–O(3)	117.0(3)	O(16)#1–Zn(5)–O(11)	124.9(5)	O(15)#1–Zn(7)–O(13)#3	113.7(3)	O(1)–Zn(9)–O(27)	101.5(3)
O(4)–Zn(2)–N(3)	96.7(3)	O(16)#1–Zn(5)–O(22)#2	110.6(5)	O(15)#2–Zn(7)–O(13)	113.7(3)	O(19)–Zn(9)–O(27)	98.1(3)
O(3)–Zn(2)–N(3)	111.0(4)	O(11)–Zn(5)–O(22)#2	123.8(3)	O(15)#1–Zn(7)–O(13)	108.4(4)	O(25)#4–Zn(9)–Zn(11)#4	79.9(3)
O(4)–Zn(2)–N(1)	111.3(3)	O(16)#1–Zn(5)–O(14)	85.4(5)	O(13)#3–Zn(7)–O(13)	99.5(4)	O(27)–Zn(10)–O(27)#4	110.0(5)
O(3)–Zn(2)–N(1)	97.6(3)	O(11)–Zn(5)–O(14)	87.5(4)	O(20)–Zn(8)–O(8)#4	153.0(6)	O(27)–Zn(10)–O(7)	106.3(4)
N(3)–Zn(2)–N(1)	124.7(3)	O(22)#2–Zn(5)–O(14)	88.8(4)	O(20)–Zn(8)–O(2)	105.9(5)	O(27)#4–Zn(10)–O(7)	105.8(5)
O(24)–Zn(3)–O(23)	119.0(3)	O(16)#1–Zn(5)–O(13)	95.3(4)	O(8)#4–Zn(8)–O(2)	98.4(5)	O(27)–Zn(10)–O(7)#4	105.8(5)
O(24)–Zn(3)–N(8)	109.9(3)	O(11)–Zn(5)–O(13)	91.1(3)	O(20)–Zn(8)–O(27)	92.3(3)	O(27)#4–Zn(10)–O(7)#4	106.3(4)
O(23)–Zn(3)–N(8)	98.1(3)	O(22)#2–Zn(5)–O(13)	92.1(3)	O(8)#4–Zn(8)–O(27)	97.7(4)	O(7)–Zn(10)–O(7)#4	122.2(9)
O(24)–Zn(3)–N(5)	96.6(3)	O(14)–Zn(5)–O(13)	178.6(4)	O(2)–Zn(8)–O(27)	93.7(3)	O(8)#4–Zn(8)–O(28)	84.9(6)
O(23)–Zn(3)–N(5)	110.6(3)	O(6)#3–Zn(6)–O(21)#2	112.9(3)	O(20)–Zn(8)–O(28)	84.1(5)	O(6)#3–Zn(6)–O(12)	103.8(4)
N(8)–Zn(3)–N(5)	124.3(3)						

Symmetry transformations used to generate equivalent atoms for **1**: #1: –x–1/2, y–3/2, –z–1; #2: x+1/2, y–3/2, z+1; #3: –x, y, –z; #4: –x, y, –z–1; #5: x–1/2, y+3/2, z–1; #6: –x–1/2, y+3/2, –z–1

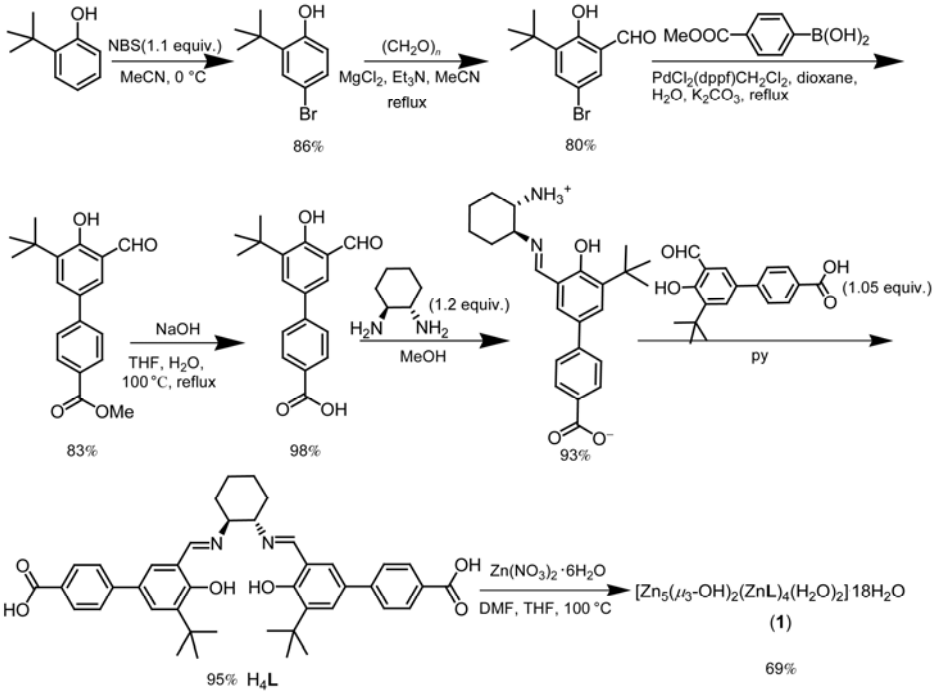

Scheme 1 Synthesis of the ligand H_4**L** and complex **1**.

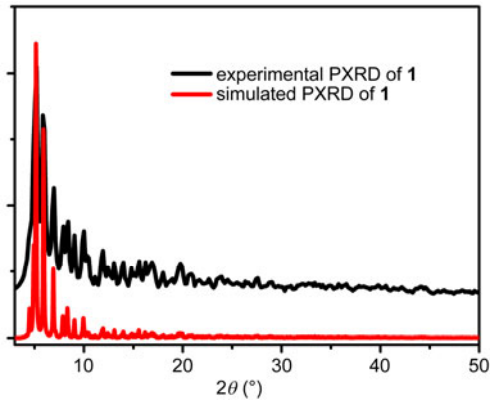

Figure 1 Experimental and simulated powder XRD patterns of **1**.

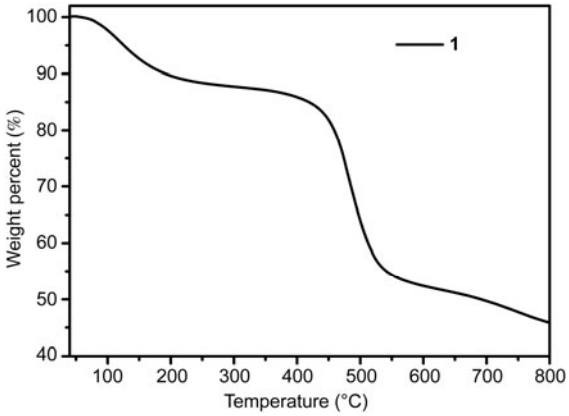

Figure 2 Thermal analysis curve of **1**.

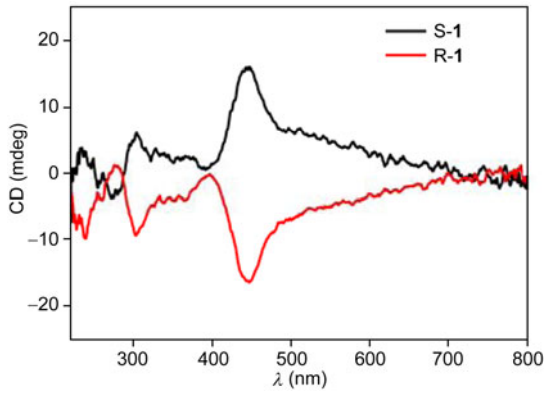

Figure 3 CD spectra of (R)/(S)-**1**.

stretching vibrations of methyl group. Solid-state circular dichroism (CD) spectra of **1** made from *R* and *S* enantiomers of the H_4**L** ligand are mirror images of each other, which indicate their enantiomeric nature (Figure 3).

3.2 Structural description

A single-crystal X-ray diffraction study performed on **1** reveals a neutral 3D open metal-organic network. **1** crystallizes in chiral monoclinic space group C_2 and the asymmetric unit contains one formular unit. The basic building unit of complex **1** is composed of a pentanuclear $[Zn_5(\mu_3\text{–}OH)_2(O_2C)_8]$ cluster and a dinuclear metallosalen $(Zn\mathbf{L})_2$. As shown in Figure 4, the pentanuclear $[Zn_5(\mu_3\text{–}OH)_2(O_2C)_8]$ unit is clustered by six bidentate and two monodentate carboxylate groups of eight Zn**L** units. Of the three independent Zn ions in the $[Zn_5(\mu_3\text{–}OH)_2(O_2C)_8]$ cluster, one (Zn7) is coordinated by two μ_3–OH^- anion and two oxygen atoms from two bidentate carboxylate groups, another (Zn6) is coordinated by one μ_3–OH^- anion and three oxygen atoms from one monodentate carboxylate group and two bidentate carboxylate groups, and the third (Zn5) is coordinated by one μ_3–OH^- anion and one water molecule and three oxygen atoms from three bidentate carboxylate groups. Thus, the Zn6 and Zn7 ions adopt a distorted tetrahedral geometry with Zn–O bond lengths ranging from 1.907(9) to 1.975(6) Å, whereas the Zn5 adopts a trigonal bipyramidal geometry with Zn–O bond lengths ranging from 1.905(7) to 2.118(7) Å.

In the two independent dimeric $(Zn\mathbf{L})_2$ units (Zn1 and Zn2, Zn3 and Zn4), each Zn center is coordinated in a distorted tetrahedral geometry with two nitrogen atoms and two oxygen atoms from two **L** ligands, which are tightly intertwisted with each other (Figure 5). The Zn–N bond lengths range from 1.970(8) Å to 2.041(8) Å and Zn–O bond lengths range from 1.883(7) to 1.911(7) Å, respectively, while the bond angles around Zn centers vary from 96.6(3) to 126.0(3)°. A careful examination of the crystal structure of **1** reveals the ligand **L** in the dimer adopts a unique conformation that significantly differs from the common monomer Zn**L** or other M**L** motifs (Scheme 2) [22, 26–28]. The $(Zn\mathbf{L})_2$ dimer acts as a multi-functionlized metalloligand and binds to two $[Zn_5(\mu_3\text{–}OH)_2(O_2C)_8]$ clusters using its four carboxylate groups.

Each pentanuclear Zn_5 cluster in **1** is thus linked by four $(Zn\mathbf{L})_2$ motifs and each $(Zn\mathbf{L})_2$ unit is linked to two $[Zn_5(\mu_3\text{–}OH)_2(O_2C)_8]$ clusters to generate a chiral porous 3D

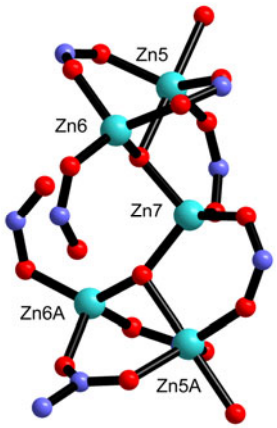

Figure 4 View of the pentanuclear $[Zn_5(\mu_3\text{–}OH)_2(O_2C)_8]$ cluster.

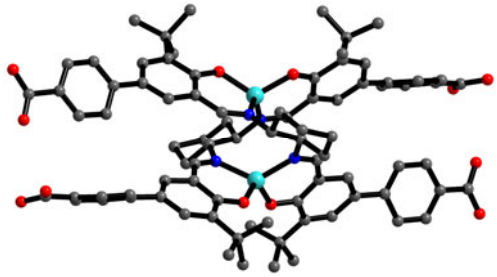

Figure 5 View of the structure of $(ZnL)_2$ dimer.

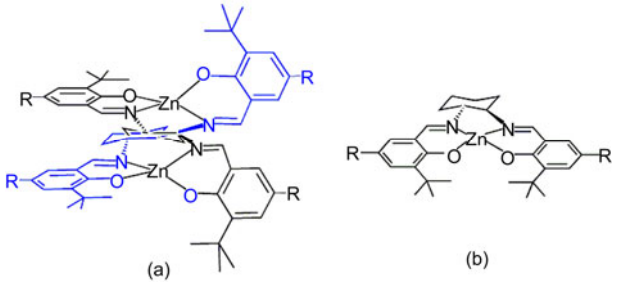

Scheme 2 View of the coordination model of the different Zn**L** units.

framework (Figure 6). The single network possesses ~2.86 nm × 2.76 nm quadrangular channel along the *a*-axis and ~4.2 nm × 2.6 nm hexagonal channel along the *c*-axis (Figures 7 and 8). The overall structure of **1** contains three identical nets of $[Zn_5(\mu_3\text{–}OH)_2(ZnL)_4(H_2O)_2]$, which are mutually interpenetrated with each other to form a 3-fold interpenetrating 3D framework. The open channels in the single network along *a* and *c*-axis are greatly reduced in the 3-fold interpenetrated framework of **1** as the pores are nearly completely occupied by $(ZnL)_2$ motifs from another two nets. Despite this, there still exists a large 1D channel of 1.14 nm × 0.58 nm along the *b* axis (Figure 9). Calculations using the PLATON program indicate that **1** has 64.5% of total volume available for guest inclusion [29].

Figure 6 The building block in **1** (the Zn atoms are shown in polyhedron).

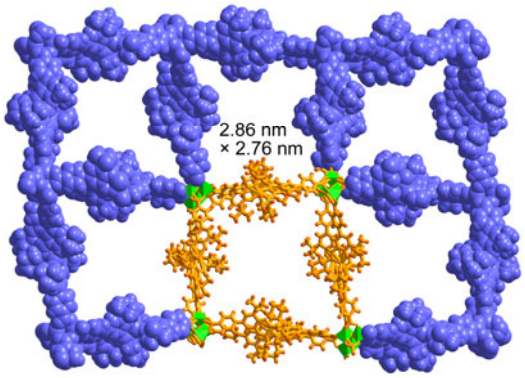

Figure 7 A view of 3D porous structure of **1** along the *a*-axis.

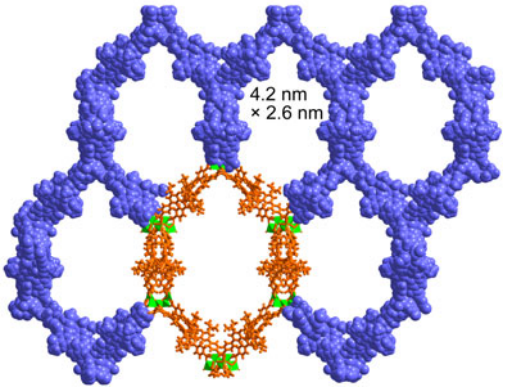

Figure 8 A view of 3D porous structure of **1** along the *c*-axis.

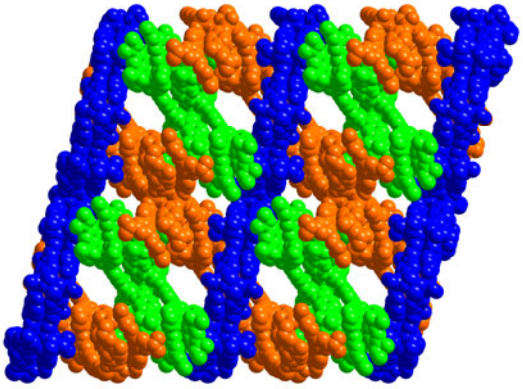

Figure 9 The space-filling representations of a 1D channel of 1.14 nm × 0.58 nm along the *b*-axis.

3.3 Photoluminescence property

The electronic spectrum of H_4L is characterized by three $\pi\rightarrow\pi^*$ transitions of phenyl and azomethine groups at 235, 263 and 318 nm, respectively. In addition, the band around 440 nm derives from the lowest absorption energy level of $\pi\rightarrow\pi^*$ transiton. Upon the formation of **1**, the two high energy bands around 263 and 318 nm show slight red shift (~7 nm), while the lowest energy band shows blue shift (~14

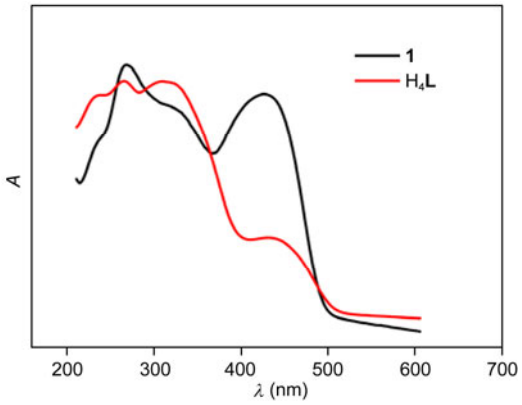

Figure 10 UV-vis absorption spectra of **1** and H_4**L** in the solid state.

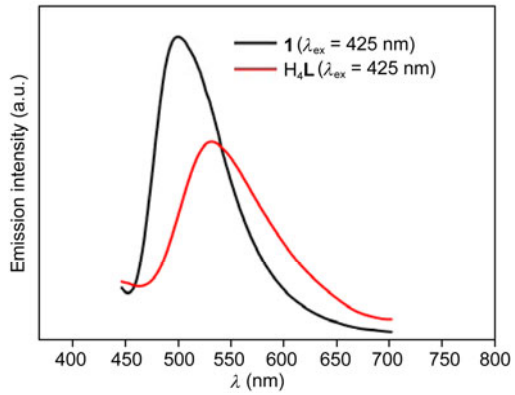

Figure 11 Fluorescent emission spectra of **1** and H_4**L**.

nm) (Figure 10). Upon excitation at 425 nm, **1** exhibits a fluorescence emission with fluorescence quantum yield of 2.5% at 500 nm. And the fluorescence spectrum of **1** shows that the emission peak is essentially the same as the solid-state fluorescence signal of free ligand but with a blue shift about 32 nm and thus can be assigned to the intraligand fluorescence emission (Figure 11).

4 Conclusions

In summary, we have synthesized one porous Zn(salen)-based metal-metallosalen framework, **1**, from a C_2-symmetric dicarboxyl-functionalized salen ligand. As expected, complex **1** exhibits a high thermal stability and good photoluminescence in the visible region.

This work was supported by the National Natural Science Foundation of China (21025103 and 21371119), the National Basic Research Program of China (973 Program, 2014CB932102 and 2012CB8217), and Shanghai Science and Technology Committee (10DJ1400100 and 12XD1406300).

1 Eddaoudi M, David BM, Li HL, Chen BL, Reineke TM, O'Keeffe M, Yaghi OM. Modular chemistry: Secondary building units as a basis for the design of highly porous and robust metal-organic carboxylate frameworks. *Acc Chem Res*, 2001, 34: 319–330
2 Qiu SL, Zhu GS. Molecular engineering for synthesizing novel structures of metal-organic frameworks with multifunctional properties. *Coord Chem Rev*, 2009, 253: 2891–2911
3 Rosi NL, Eckert J, Eddaoudi M, Vodak DT, Kim J, O'Keeffe M, Yaghi OM. Hydrogen storage in microporous metal-organic frameworks. *Science,* 2003, 300: 1127–1129
4 Lee JY, Farha OK, Roberts J, Scheidt KA, Nguyen ST, Hupp JT. Metal-organic framework materials as catalysts. *Chem Soc Rev*, 2009, 38: 1450–1459
5 Murray LJ, Dincă M, Long JR. Hydrogen storage in metal-organic frameworks. *Chem Soc Rev*, 2009, 38: 1294–1314
6 Chen B, Xiang S, Qian, G. Metal-organic frameworks with functional pores for recognition of small molecules. *Acc Chem Res,* 2010, 43: 1115–1124
7 Li JR, Kuppler RJ, Zhou HC. Selective gas adsorption and separation in metal-organic frameworks. *Chem Soc Rev*, 2009, 38: 1477–1504
8 Allendorf MD, Bauer CA, Bhakta RK, Houk RJT. Luminescent metal-organic frameworks. *Chem Soc Rev*, 2009, 38: 1330–1352
9 Cui Y, Yue Y, Qian G, Chen B. Luminescent functional metal-organic frameworks. *Chem Rev,* 2011, 112: 1126–1162
10 Cao AM, Hu JS, Wan LJ. Morphology control and shape evolution in 3D hierarchical superstructures. *Sci China Chem*, 2012, 55: 2249–2256
11 Ma L, Abney C, Lin W. Enantioselective catalysis with homochiral metal-organic frameworks. *Chem Soc Rev,* 2009, 38: 1248–1256
12 Ma L, Falkowski JM, Abney C, Lin W. A series of isoreticular chiral metal-organic frameworks as a tunable platform for asymmetric catalysis. *Nat Chem,* 2010, 2: 838–846
13 Xuan W, Zhu C, Liu Y, Cui Y. Mesoporous metal-organic framework materials. *Chem Soc Rev,* 2012, 41: 1677–1695
14 Furukawa H, Ko N, Go YB, Aratani N, Choi SB, Choi E, Yazaydin AÖ, Snurr RQ, O'Keeffe M, Kim J, Yaghi OM. Ultrahigh porosity in metal-organic frameworks. *Science,* 2010, 329: 424–428
15 Zhao D, Timmons DJ, Yuan D, Zhou HC. Tuning the topology and functionality of metal-organic frameworks by ligand design. *Acc Chem Res,* 2010, 44: 123–133
16 Cho S-H, Ma B, Nguyen ST, Hupp JT. Albrecht-Schmitt TE. A metal-organic framework material that functions as an enantioselective catalyst for olefin epoxidation. *Chem Comm,* 2006, 24: 2563–2565
17 Shultz AM, Sarjeant AA, Farha OK, Hupp JT, Nguyen ST. Post-synthesis modification of a metal-organic framework to form metallosalen-containing MOF materials. *J Am Chem Soc,* 2011, 133: 13252–13255
18 Song F, Wang C, Falkowski JM, Ma L, Lin W. Isoreticular chiral metal-organic frameworks for asymmetric alkene epoxidation: Tuning catalytic activity by controlling framework catenation and varying open channel sizes. *J Am Chem Soc,* 2010, 132: 15390–15398
19 Yuan G, Zhu C, Liu Y, Cui Y. Nano- and microcrystals of a Mn-based metal-oligomer framework showing size-dependent magnetic resonance behaviors. *Chem Comm,* 2011, 47: 3180–3182
20 Li G, Yu WB, N J, Liu TF, Liu Y, Sheng EH, Cui Y. Self-assembly of a homochiral nanoscale metallacycle from a metallosalen complex for enantioselective separation. *Angew Chem Int Ed,* 2008, 47: 1245–1249
21 Li G, Yu W, Cui Y. A homochiral nanotubular crystalline framework of metallomacrocycles for enantioselective recognition and separation. *J Am Chem Soc,* 2008, 130: 4582–4583
22 Zhu C, Yuan G, Chen X, Yang Z, Cui Y. Chiral nanoporous metal-metallosalen frameworks for hydrolytic kinetic resolution of epoxides. *J Am Chem Soc,* 2012, 134: 8058–8061
23 Zhu C, Xuan W, Cui Y. Luminescent microporous metal-metallo-

salen frameworks with the primitive cubic net. *Dalton Trans,* 2012, 41: 3928–3932
24 Sheldrick GM. SHELXTL Version 5.1 Software reference manual. Madison, Wisconsin: Bruker AXS, Inc., 1997
25 Jeon YM, Heo J, Mirkin CA. Acid-functionalized dissymmetric salen ligands and their manganese(III) complexes. *Tetrahedron Lett,* 2007, 48: 2591–2595
26 Jeon YM, Heo J, Mirkin CA. Dynamic interconversion of amorphous microparticles and crystalline rods in salen-based homochiral infinite coordination polymers. *J Am Chem Soc,* 2007, 129: 7480–7481
27 Heo J, Jeon, YM, Mirkin CA. Reversible interconversion of homochiral triangular macrocycles and helical coordination polymers. *J Am Chem Soc,* 2007, 129: 7712–7713
28 Germain ME, Vargo TR, McClure BA, Rack JJ, Van Patten PG, Odoi M, Knapp MJ. Quenching Mechanism of Zn(Salicylaldimine) by Nitroaromatics. *Inorg Chem,* 2008, 47: 6203–6211
29 Spek AL. PLATON, Version 1.62. Utrecht, Nederland: University of Utrecht, 1999